Unsteady Pulsatile Flow through a Vertical Constricted Annulus with Heat Transfer

Yasser Abd elmaboud[a,b] and Khaled Saad Mekheimer[c]

[a] Mathematics Department, Faculty of Science and Arts, Khulais, King Abdulaziz University (KAU), Saudi Arabia

[b] Mathematics Department, Faculty of Science, Al-Azhar University (Assiut Branch), Assiut, Egypt

[c] Mathematics Department, Faculty of Science, Al-Azhar University, Nasr City, 11884 Cairo, Egypt

Reprint requests to Y. A.; E-mail: yass_math@yahoo.com

Z. Naturforsch. **67a,** 185 – 194 (2012) / DOI: 10.5560/ZNA.2012-0011
Received May 22, 2011 / revised December 7, 2011

This paper investigates the effects of heat transfer and pulsatile flow of a Newtonian fluid (blood) through a vertical annulus with mild constriction on the outer wall while the inner wall represents the catheter tube. An analytical expression in terms of Bessel functions of the first and second kind is obtained for the heat and the velocity components. The variation of pressure gradient with steady flow rate is given as well as the wall shear stress distribution for different values of time. The pressure gradient and the wall shear stress are calculated, and their variations are discussed with respect to the Grashof number, the height of the constriction, and the size of the catheter. It is observed that an increase in the catheter size increases the pressure gradient as well as the wall shear stress.

Key words: Pulsatile Flow; Heat Transfer; Catheter; Stenosed Arteries.

1. Introduction

In the recent times, cardiac catheterization considers an important medical diagnostic tool that allows a comprehensive examination of the heart and surrounding blood vessels. It enables the physician to take angiograms, record blood flow, calculate cardiac output and vascular resistance, perform an endomyocardial biopsy, and evaluate the heart's electrical activity. Cardiac catheterization is performed by inserting one or more catheters (thin flexible tubes) through a peripheral blood vessel in the arm or leg under X-ray guidance. The insertion of a catheter in an artery will alter the flow field and modify the pressure distribution [1]. Coronary catheter probes (e.g. intravascular pressure probes and intravascular ultrasound probes) are widely used as they provide valuable information about arterial anatomy and the hemodynamic significance of stenoses. Current noninvasive techniques for measurement of anatomy and hemodynamics, such as magnetic resonance imaging (MRI) and transthoracic ultrasound, lack adequate resolution in coronary arteries. Recently, coronary catheter probes have also been used in conjunction with computational fluid dynamics (CFD) to study the relationship between flow patterns and atheroma formation, for which accurate measurement of velocity is crucial [2].

Artificial circulatory devices represent an indispensable aid in clinical practice by using vascular access methods (performed by the insertion of cannula into vessels). The insertion of cannula into vessels may disturb the physiological flow of blood, giving rise to non-physiological pressure variations and shear stresses [3].

Circulatory system disorders are known to be responsible in most cases of death, and stenosis or arteriosclerosis is one such cause. Stenosis, a medical term which means narrowing of any body passage, tube or orifice, is the abnormal and unnatural growth in arterial wall thickness that develops at various locations of the cardiovascular system under diseased conditions. This can cause circulatory disorders by reducing or occluding the blood supply which may result in serious consequences. An account of the important contributions to the topic may be had from Shukla et al. [4] and Srivastava [5]. The study of the stenosis effect is im-

portant because once a mild stenosis is developed, the resulting flow will be disordered, furthermore, changes the regional blood rheology. Mathematical modelling of blood flow through a stenosed tube was studied by many authors. Many authors have dealt with this problem treating blood as a Newtonian or non-Newtonian fluid [5 – 18].

Heat transfer analysis can be used to obtain information about the properties of tissues. For example, the flow of blood can be evaluated using a dilution technique. In this procedure, heat is either injected or generated locally and the thermal clearance is monitored. With knowledge of initial thermal conditions and the thermal clearance rate, it is possible to estimate blood flow rates.

The purpose of this paper is to investigate the effect of unsteady pulsatile blood flow through a vertical annulus with mild constriction at the outer wall while the inner wall represents the catheter tube. Furthermore, we study the effects of heat transfer and catheterization on various physiologically important flow characteristics. The problem is first modelled and then solved analytically for the velocity, the temperature, and the axial pressure gradient. A motivation of the present analysis is the hope that such a problem will be applicable in many clinical applications such as transport of fluid in arterioles.

2. Mathematical Model

Let us consider the laminar pulsatile flow of blood through the gap between two coaxial vertical tubes. The inner tube (catheter) is rigid maintained at a temperature T_2', and the outer treated as a long elastic tube having a stenosis in its lumen, and it is exposed to a temperature T_1' (see Fig. 1). Assume that the stenosis over a length of the artery being assumed to have developed in an axisymmetric manner. The catheter and the stenosis walls are defined as

$$R_1' = a_1', \tag{1}$$

$$R_2'(z') = \begin{cases} R_0' - \dfrac{\delta}{2}\left[1+\cos\left(\dfrac{\pi z'}{z_0'}\right)\right], & -z_0' \le z' \le z_0', \\ R_0', & \text{otherwise.} \end{cases} \tag{2}$$

The problem has been studied in a cylindrical coordinate system (r', z'), where the z'-axis is taken along the axis of the artery (vertical) while r' is taken along the radial. We assume that the geometry is axisymmetric. Hence the flow velocity vector is given by

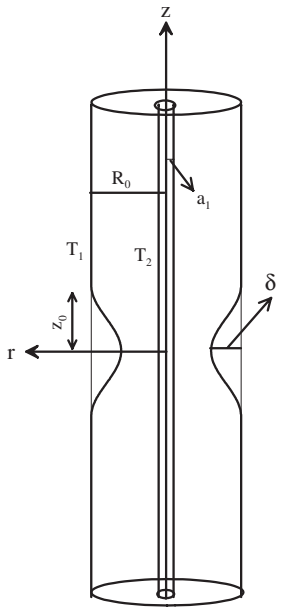

Fig. 1. Geometry of the problem.

$\mathbf{q}'^* = (u'^*(r',z',t'), w'^*(r',z',t'))$. The equations governing the problem are

$$\frac{\partial u'^*}{\partial r'} + \frac{\partial w'^*}{\partial z'} + \frac{u'^*}{r'} = 0, \tag{3}$$

$$\rho\left[\frac{\partial u'^*}{\partial t'} + u'^*\frac{\partial u'^*}{\partial r'} + w'^*\frac{\partial u'^*}{\partial z'}\right] = -\frac{\partial p'^*}{\partial r'} + \mu\left[\frac{\partial^2 u'^*}{\partial r'^2} + \frac{1}{r'}\frac{\partial u'^*}{\partial r'} + \frac{\partial^2 u'^*}{\partial z'^2} - \frac{u'^*}{r'^2}\right], \tag{4}$$

$$\rho\left[\frac{\partial w'^*}{\partial t'} + u'^*\frac{\partial w'^*}{\partial r'} + w'^*\frac{\partial w'^*}{\partial z'}\right] = -\frac{\partial p'^*}{\partial z'} + \mu\left[\frac{\partial^2 w'^*}{\partial r'^2} + \frac{1}{r'}\frac{\partial w'^*}{\partial r'} + \frac{\partial^2 w'^*}{\partial z'^2}\right] + \rho g\alpha(T' - T_s), \tag{5}$$

and the energy equation

$$\rho c_p\left[\frac{\partial T'^*}{\partial t'} + u'^*\frac{\partial T'^*}{\partial r'} + w'^*\frac{\partial T'^*}{\partial z'}\right] = k\left[\frac{\partial^2 T'^*}{\partial r'^2} + \frac{1}{r'}\frac{\partial T'^*}{\partial r'} + \frac{\partial^2 T'^*}{\partial z'^2}\right] + Q_0(T' - T_s). \tag{6}$$

Under the assumptions and simplifications discussed in Srivastava and Srivastava [19], along with the conditions in Young [20], it can be shown that the radial velocity is negligibly small and can be neglected for

a low Reynolds number flow in a tube with mild stenosis. The appropriate equations describing the unsteady fluid flow in the case of a mild stenosis ($\delta \ll R_0'$) can be set in the form

$$0 = -\frac{\partial p'^*}{\partial r'}, \tag{7}$$

$$\rho \frac{\partial w'^*}{\partial t'} = -\frac{\partial p'^*}{\partial z'} + \mu\left[\frac{\partial^2 w'^*}{\partial r'^2} + \frac{1}{r'}\frac{\partial w'^*}{\partial r'}\right] + \rho g\alpha(T' - T_s), \tag{8}$$

the energy equation

$$\rho c_p \frac{\partial T'^*}{\partial t'} = k\left[\frac{\partial^2 T'^*}{\partial r'^2} + \frac{1}{r'}\frac{\partial T'^*}{\partial r'}\right] + Q_0(T' - T_s). \tag{9}$$

The corresponding boundary conditions are

$$\begin{aligned} &w'^* = 0,\ T'^* = T_2 \ \text{ at } \ r' = R_1', \\ &w'^* = 0,\ T'^* = T_1 \ \text{ at } \ r' = R_2'. \end{aligned} \tag{10}$$

Consider the following non-dimensional variables and parameters:

$$\begin{aligned} &z = \frac{z'}{R_0},\ r = \frac{r'}{R_0},\ w^* = \frac{w'^*}{u_0},\ t = \Omega t',\ p^* = \frac{R_0}{\mu u_0}p'^*, \\ &r_1 = \frac{R_1'}{R_0} = a,\ r_2 = \frac{R_2'}{R_0},\ \varepsilon = \frac{\delta}{R_0},\ z_0 = \frac{z_0'}{R_0}, \\ &\alpha^2 = \frac{\rho\Omega R_0^2}{\mu},\ \theta^* = \frac{T'^* - T_s}{T_1 - T_s},\ \beta = \frac{Q_0 R_0^2}{k(T_1 - T_s)}, \\ &\mathrm{Pr} = \frac{\mu c_p}{k},\ \mathrm{Gr} = \frac{\rho g\alpha R_0^2(T_1 - T_s)}{\mu u_0}. \end{aligned} \tag{11}$$

With the help of (11), the non-dimensional equations for (1), (2), (7)–(9) will be

$$r_1 = a, \tag{12}$$

$$r_2(z) = \begin{cases} 1 - \dfrac{\varepsilon}{2}\left[1 + \cos\left(\dfrac{\pi z}{z_0}\right)\right], & -z_0 \le z \le z_0, \\ 1, & \text{otherwise}, \end{cases} \tag{13}$$

$$0 = -\frac{\partial p^*}{\partial r}, \tag{14}$$

$$\alpha^2 \frac{\partial w^*}{\partial t} = -\frac{\partial p^*}{\partial z} + \left[\frac{\partial^2 w^*}{\partial r^2} + \frac{1}{r}\frac{\partial w^*}{\partial r}\right] + \mathrm{Gr}\theta^*, \tag{15}$$

the energy equation

$$\alpha^2 \mathrm{Pr}\frac{\partial \theta^*}{\partial t} = k\left[\frac{\partial^2 \theta^*}{\partial r^2} + \frac{1}{r}\frac{\partial \theta^*}{\partial r}\right] + \beta. \tag{16}$$

Equation (14) shows that the pressure gradient is a function of z and t only. The corresponding non-dimensional boundary conditions are

$$\begin{aligned} &w^* = 0,\ \theta^* = m \ \text{ at } \ r = R_1 = a, \\ &w^* = 0,\ \theta^* = 1 \ \text{ at } \ r = R_2, \end{aligned} \tag{17}$$

where $m = \frac{T_2 - T_s}{T_1 - T_s}$ is the wall temperature ratio. In addition to the above boundary conditions, we have the condition that the pressure p is p_1 at $z = -L$ and p_2 at $z = L$.

3. Solution Development

Since the flow is pulsatile of circular frequency Ω, we seek a solution of the non-dimensional form $w^* = w(r,z)\,\mathrm{e}^{\mathrm{i}t}$, $P^* = P(z)\,\mathrm{e}^{\mathrm{i}t}$, $\theta^* = \theta(r,z)\,\mathrm{e}^{\mathrm{i}t}$. Equations (15) and (16) can be simplified to the form

$$w_{rr} + \frac{1}{r}w_r - \alpha_2^2 w = -\frac{\mathrm{d}p}{\mathrm{d}z} - \mathrm{Gr}\theta, \tag{18}$$

$$\theta_{rr} + \frac{1}{r}\theta_r - \alpha_1^2\theta = -\beta, \tag{19}$$

where $\alpha_1^2 = \mathrm{i}\,\alpha^2\mathrm{Pr}$ and $\alpha_2^2 = \mathrm{i}\,\alpha^2$. The solution of (19) is

$$\theta(r,z) = C_1 I_0(\alpha_1 r) + C_2 K_0(\alpha_1 r) + \frac{\beta}{\alpha_1}, \tag{20}$$

where I_0 and K_0 are the modified Bessel functions of the zeroth-order first and second kind, respectively. C_1 and C_2 are arbitrary functions of z. Using the non-dimensional boundary conditions (17), we can obtain the values of C_1, C_2 in the form

$$C_1 = \frac{\beta[K_0(a\alpha_1) - K_0(R_2\alpha_1)] + \alpha_1^2[mK_0(R_2\alpha_1) - K_0(a\alpha_1)]}{\alpha_1^2[I_0(a\alpha_1)K_0(R_2\alpha_1) - I_0(R_2\alpha_1)K_0(a\alpha_1)]},$$

$$C_2 = -\frac{\left(\frac{\beta}{\alpha_1^2 - m}\right)I_0(R_2\alpha_1) - \left(\frac{\beta}{\alpha_1^2} - 1\right)I_0(a\alpha_1)}{[I_0(R_2\alpha_1)K_0(a\alpha_1) - I_0(a\alpha_1)K_0(R_2\alpha_1)]}.$$

Substitute from (20) into (18), the solution of (18) is

$$w(r,z) = I_0(r\alpha_2)C_3 + K_0(r\alpha_2)C_4 + \frac{P_z}{\alpha_2^2} + \frac{\mathrm{Gr}\beta}{\alpha_1^2\alpha_2^2} - \frac{\mathrm{Gr}[C_1 I_0(r\alpha_1) + C_2 K_0(r\alpha_1)]}{\alpha_1^2 - \alpha_2^2}. \tag{21}$$

Using the non-dimensional boundary conditions (17), we can obtain the values of C_3, C_4 in the form

$$C_3 = \Big\{ K_0(a\alpha_2)\Big(\mathrm{Gr}\alpha_1^2\alpha_2^2(C_1I_0(R_2\alpha_1)+C_2K_0(R_2\alpha_1)) - (\alpha_1^2-\alpha_2^2)(P_z\alpha_1^2+\mathrm{Gr}\beta)\Big) + K_0(R\alpha_2)\Big((\alpha_1^2-\alpha_2^2)(P_z\alpha_1^2+\mathrm{Gr}\beta) - \mathrm{Gr}\alpha_1^2\alpha_2^2(C_1I_0(a\alpha_1)+C_2K_0(a\alpha_1))\Big)\Big\} \cdot \frac{1}{(\alpha_1^2(\alpha_1-\alpha_2)\alpha_2^2(\alpha_1+\alpha_2)(I_0(R\alpha_2)K_0(a\alpha_2)-I_0(a\alpha_2)K_0(R\alpha_2)))},$$

$$C_4 = \frac{1}{I_0(a\alpha_2)K_0(R_2\alpha_2)-I_0(R_2\alpha_2)K_0(a\alpha_2)}\left\{ I_0(R_2\alpha_2)\left(\frac{\left(P_z+\frac{\mathrm{Gr}\beta}{\alpha_1^2}\right)}{\alpha_2^2} - \frac{\mathrm{Gr}(C_1I_0(a\alpha_1)+C_2K_0(a\alpha_1))}{\alpha_1^2-\alpha_2^2}\right) + I_0(a\alpha_2)\left(\frac{\left(P_z+\frac{\mathrm{Gr}\beta}{\alpha_1^2}\right)}{\alpha_2^2} - \frac{\mathrm{Gr}(C_1I_0(R_2\alpha_1)+C_2K_0(R_2\alpha_1))}{\alpha_1^2-\alpha_2^2}\right)\right\},$$

where $P_z = \frac{\mathrm{d}p}{\mathrm{d}z}$. The non-dimensional steady state flow rate Q_s is given by

$$Q_\mathrm{s} = 2\int_a^{R_2} rw(r,z)\,\mathrm{d}r = \frac{P_z(R_2^2-a^2)}{\alpha_2^2} + \frac{\mathrm{Gr}\beta(R_2^2-a^2)}{\alpha_1^2\alpha_2^2} + \frac{2C_1\mathrm{Gr}(aI_1(a\alpha_1)-R_2I_1(R_2\alpha_1))}{\alpha_1^3-\alpha_1\alpha_2^2} + \frac{2C_3(R_2I_1(R_2\alpha_2)-aI_1(a\alpha_2))}{\alpha_2} + \frac{2C_2\mathrm{Gr}(R_2K_1(R_2\alpha_1)-aK_1(a\alpha_1))}{\alpha_1^3-\alpha_1\alpha_2^2} + \frac{2C_4(aK_1(a\alpha_2)-R_2K_1(R_2\alpha_2))}{\alpha_2}. \tag{22}$$

Using the expressions of C_3 and C_4 in (22), we can find the axial pressure gradient in the form

$$\begin{aligned}\frac{\mathrm{d}p}{\mathrm{d}z} = \Bigg\{ & -Q_\mathrm{s} + \frac{\beta\mathrm{Gr}(R_2^2-a^2)}{\alpha_1^2\alpha_2^2} + \frac{2C_1\mathrm{Gr}(aI_1(a\alpha_1)-R_2I_1(R_2\alpha_1))}{\alpha_1^3-\alpha_1\alpha_2^2} \\ & + \frac{2\mathrm{Gr}\beta(\alpha_2-\alpha_1)(R_2I_1(R_2\alpha_2)-aI_1(a\alpha_2))K_0(a\alpha_2)}{\alpha_1^2(\alpha_1-\alpha_2)\alpha_2^3a_{11}} \\ & + \frac{2\mathrm{Gr}(-aI_1(a\alpha_2)+R_2I_1(R_2\alpha_2))(C_1I_0(R_2\alpha_1)+C_2K_0(R_2\alpha_1))K_0(a\alpha_2)}{(\alpha_1-\alpha_2)\alpha_2(\alpha_1+\alpha_2)a_{11}} \\ & + \frac{2\mathrm{Gr}\beta(-aI_1(a\alpha_2)+R_2I_1(R_2\alpha_2))K_0(R_2\alpha_2)}{\alpha_1^2\alpha_2^3a_{11}} + \frac{2C_2\mathrm{Gr}(-aK_1(a\alpha_1)+R_2K_1(R_2\alpha_1))}{\alpha_1^3-\alpha_1\alpha_2^2} \\ & - \frac{2\mathrm{Gr}(-aI_1(a\alpha_2)+R_2I_1(R_2\alpha_2))(C_1I_0(a\alpha_1)+C_2K_0(a\alpha_1))K_0(R_2\alpha_2)}{(\alpha_1-\alpha_2)\alpha_2(\alpha_1+\alpha_2)a_{11}} \\ & + \frac{2\mathrm{Gr}\beta I_0(a\alpha_2)(aK_1(a\alpha_2)-R_2K_1(R_2\alpha_2))}{\alpha_1^2\alpha_2^3a_{11}} - \frac{2\mathrm{Gr}\beta I_0(R_2\alpha_2)(aK_1(a\alpha_2)-R_2K_1(R_2\alpha_2))}{\alpha_1^2\alpha_2^3a_{11}} \\ & + \frac{2\mathrm{Gr}I_0(R_2\alpha_2)(C_1I_0(a\alpha_1)+C_2K_0(a\alpha_1))(aK_1(a\alpha_2)-R_2K_1(R_2\alpha_2))}{\alpha_2(\alpha_1^2-\alpha_2^2)a_{11}} \\ & - \frac{2\mathrm{Gr}I_0(a\alpha_2)(C_1I_0(R_2\alpha_1)+C_2K_0(R_2\alpha_1))(aK_1(a\alpha_2)-R_2K_1(R_2\alpha_2))}{\alpha_2(\alpha_1^2-\alpha_2^2)a_{11}}\Bigg\} \\ & \Big/\left\{\frac{a^2-R_2^2}{\alpha_2^2} - \frac{2(\alpha_2-\alpha_1)(-aI_1(a\alpha_2)+R_2I_1(R_2\alpha_2))K_0(a\alpha_2)}{(\alpha_1-\alpha_2)\alpha_2^3a_{11}}\right.\end{aligned} \tag{23}$$

$$- \frac{2(-aI_1(a\alpha_2)+R_2I_1(R_2\alpha_2))K_0(R_2\alpha_2)}{\alpha_2^3 a_{11}} - \frac{2I_0(a\alpha_2)(aK_1(a\alpha_2)-R_2K_1(R_2\alpha_2))}{\alpha_2^3 a_{11}}$$
$$+ \frac{2I_0(R_2\alpha_2)(aK_1(a\alpha_2)-R_2K_1(R_2\alpha_2))}{\alpha_2^3 a_{11}} \Bigg\},$$

where $a_{11} = I_0(R_2\alpha_2)K_0(a\alpha_2) - I_0(a\alpha_2)K_0(R_2\alpha_2)$.

The pressure drop Δp along the annulus is obtained from (23) as

$$\Delta p = -\int_{-1}^{1} \frac{\mathrm{d}p}{\mathrm{d}z}\,\mathrm{d}z. \tag{24}$$

The dimensionless shear stress at the outer wall and resistance to the flow (resistive impedance) are given by

$$\tau_w = -\frac{\partial w}{\partial r}\bigg|_{r=R_2}, \tag{25}$$

$$\Lambda = \frac{\Delta p}{Q_s}. \tag{26}$$

The numerical integration package in the Mathematica program is used to calculate the integration in (26). Some special cases can be obtained: when $\varepsilon \to 0$, we get the analysis for straight annulus in all the above cases. Also when $\varepsilon \to 0$ and $a \to 0$, we get the analysis for straight tube in all the above cases. The type of boundary conditions used in this problem to solve the energy equation differs from those usually used in plane Poiseuille flow. The case $m = -1$ physically means that the average of the temperatures of the two walls is equal to that of the static fluid, and when $m = 2$, the wall temperatures are unequal.

4. Graphical Results and Discussion

The change in the flow pattern and the effect of heat transfer on the blood flow in a narrow artery (having a stenosis) are studied when a catheter is inserted into the artery and the flow is pulsatile.

The influences of various emerging parameters of our analysis on the axial pressure gradient $\frac{\mathrm{d}p}{\mathrm{d}z}$ are displayed in Figures 2–5. The effect of the heat source parameter β and the Grashof number Gr on the axial pressure gradient $\frac{\mathrm{d}p}{\mathrm{d}z}$ is shown in Figure 2. We noticed that the pressure gradient decreases by increasing each of β and Gr. The figure also shows that the pressure gradient is constant at the inlet and increases gradually to the maximum value at the center of the stenosis at $z = 0$, then decreases gradually and becomes constant at the outlet. Figure 3, depicts the variation of $\frac{\mathrm{d}p}{\mathrm{d}z}$ versus z for different values of the maximum height of the stenosis ε and the catheter radius a. It is clear that the pressure gradient $\frac{\mathrm{d}p}{\mathrm{d}z}$ increases by increasing the catheter radius a. Moreover, it increases as the maximum height of the stenosis ε increases in the stenosis domain. Also it shows the special case of our problem when the fluid flows in the gap between the two coaxial tubes, $\varepsilon = 0$: in such a case the pressure gradient $\frac{\mathrm{d}p}{\mathrm{d}z}$ is steady along the annulus. From Figure 4, we observe that as m decreases, the pressure gradient $\frac{\mathrm{d}p}{\mathrm{d}z}$ increases but as the steady-state flow rate Q_s increases, the pressure gradient $\frac{\mathrm{d}p}{\mathrm{d}z}$ increases. The influences of the Prandtl number Pr and the pulsatile Reynolds number (or generalized Wormersly frequency parameter) α on the variation of $\frac{\mathrm{d}p}{\mathrm{d}z}$ is shown in Figure 5. The figure shows that the effect of Pr on $\frac{\mathrm{d}p}{\mathrm{d}z}$ is negligible when $\alpha < 0.3$, but the distinct variation is noted when $\alpha \geq 0.3$, also, as the Pr increases the $\frac{\mathrm{d}p}{\mathrm{d}z}$ increments. Moreover, $\frac{\mathrm{d}p}{\mathrm{d}z}$ rises by increasing the pulsatile Reynolds number α.

The influences of various emerging parameters of our analysis on the resistance to the flow (resistive impedance) Λ are illustrated in Figures 6–8. In Figure 6 the effects of ε and a on Λ are shown. It is clear that increasing both parameters ε and a leads to a decreasing Λ in the interval $-1 \leq z < 0$ and vice versa in the interval $0 < z \leq 1$. But the important observation here is that the impedance Λ vanishes at the center of the stenosis at $z = 0$. The variation of impedance Λ versus ε for different values of β and Gr is shown in Figure 7. The figure illustrates that the impedance Λ increases by increasing the maximum height of the stenosis ε, but it decreases by increasing values of β and Gr. The variation of the impedance Λ increases as the length of the stenosis $2z_0$ and the pulsatile Reynolds number α increase as shown in Figure 8.

The influences of various emerging parameters of our analysis on the wall shear stress τ_w are illustrated in Figures 9–12. In Figure 9 the effect of the length

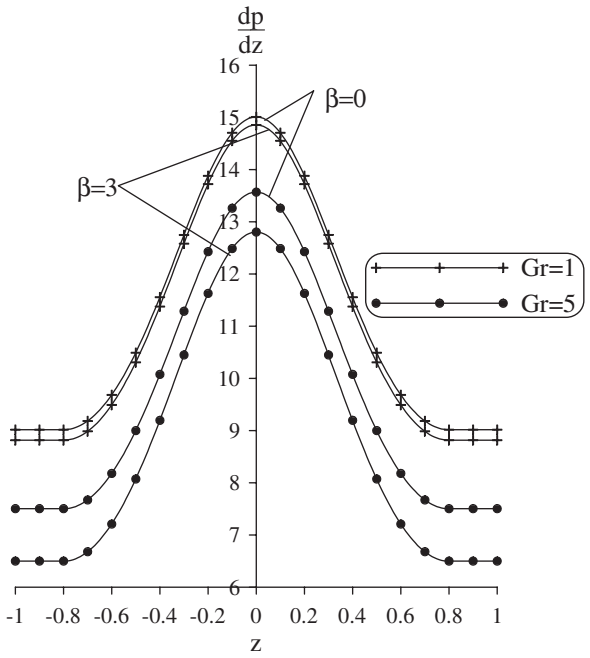

Fig. 2. Variation of pressure gradient versus z for different values of Gr and β at $a = 0.2$, $\varepsilon = 0.1$, $m = -1$, $z_0 = 0.8$, $Q_s = 0.5$, $\alpha = 0.5$, and Pr = 5.

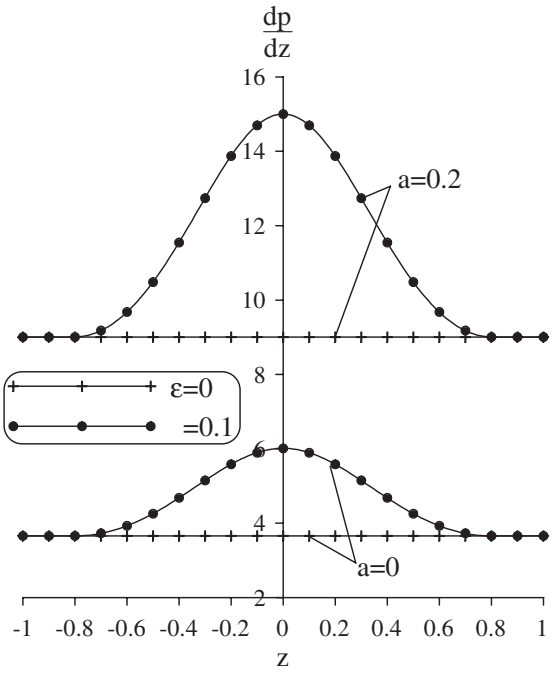

Fig. 3. Variation of pressure gradient versus z for different values of a and ε at Gr = 1, $\beta = 0.1$, $m = -1$, $z_0 = 0.8$, $Q_s = 0.5$, $\alpha = 0.5$, and Pr = 5.

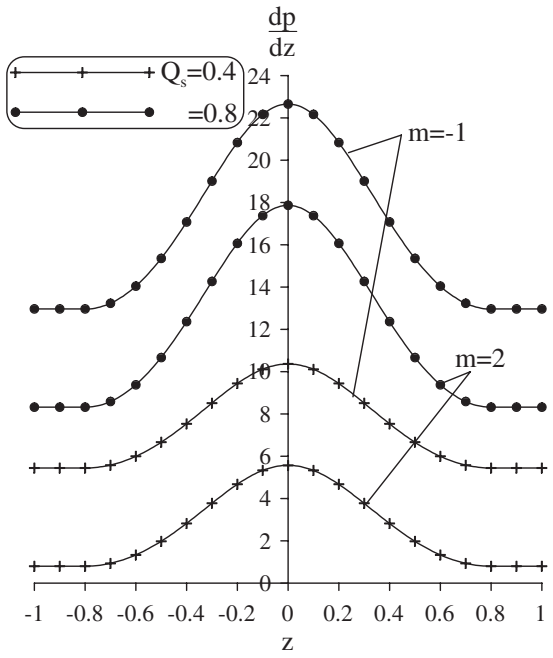

Fig. 4. Variation of pressure gradient versus z for different values of m and Q_s at Gr = 5, $\beta = 0.5$, $a = 0.2$, $z_0 = 0.8$, $\varepsilon = 0.1$, $\alpha = 0.2$, and Pr = 5.

of the stenosis $2z_0$ on the wall shear stress τ_w is shown. The figure shows that τ_w is constant in the non-stenosis part but in the stenosis part it increases to the maximum value at $z = 0$. Also the wall shear stress τ_w increases by increasing the length of the stenosis $2z_0$. Figure 10 depicts the variation of τ_w with z for different values of ε and a. The figure illustrates that the wall shear stress τ_w increases as ε and a increase. Moreover, in absent of the stenosis height ($\varepsilon = 0$) the wall shear stress is steady along the annulus. The wall shear stress τ_w decreases by increasing Gr as shown in Figure 11. The variation of the wall shear stress in a cycle of oscillation for different values of the wall temperature ratio m is shown in Figure 12. The wall shear stress decreases as t increases from 0° to 180° and increases as t increases from 90° to 360°. The figure also shows that as m increases, τ_w decreases from 0° to 90° and from 270° to 360° but it increases by increasing m from 90° to 270°. The influences of various emerging parameters of our analysis on the temperatures θ of the fluid are illustrated in Figures 13 – 15. The effects of the heat source parameter β and the wall temperature ratio m on the temperatures θ of the fluid is shown in Figure 13. It is noticed that the heat decreases from its value $m = 2$

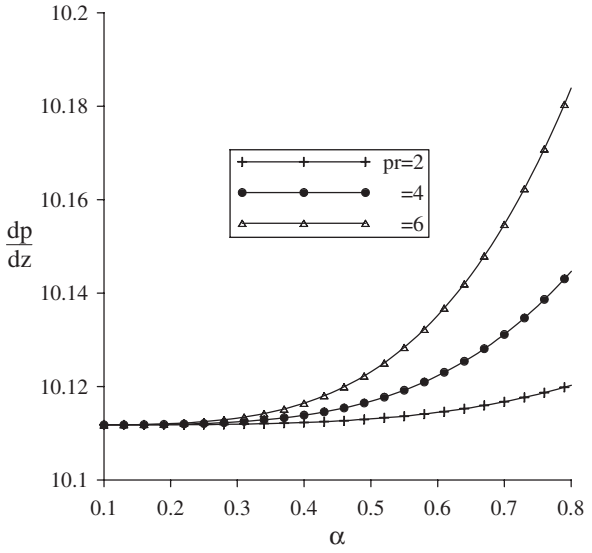

Fig. 5. Variation of pressure gradient versus α for different values of Pr at Gr $= 5$, $\beta = 0.5$, $a = 0.2$, $z_0 = 0.8$, $\varepsilon = 0.1$, $z = 0.1$, $Q_s = 0.4$, and $m = -1$.

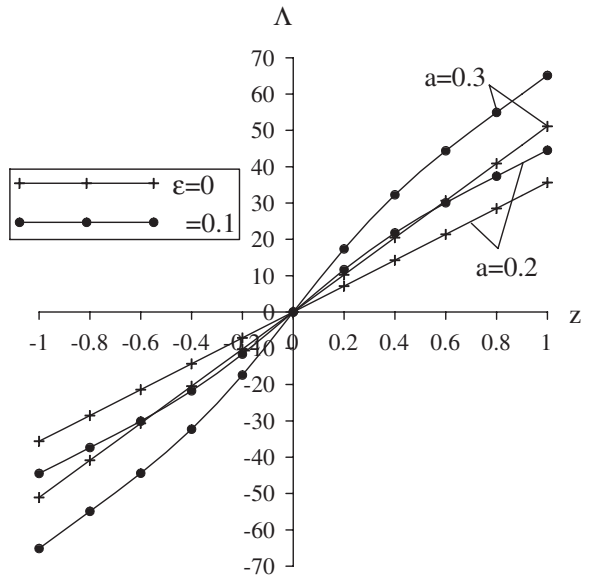

Fig. 6. Variation of longitudinal impedance versus z for different values of a and ε at Gr $= 1$, $\beta = 0.1$, $m = -1$, $z_0 = 0.8$, $Q_s = 0.4$, $\alpha = 0.4$, and Pr $= 2$.

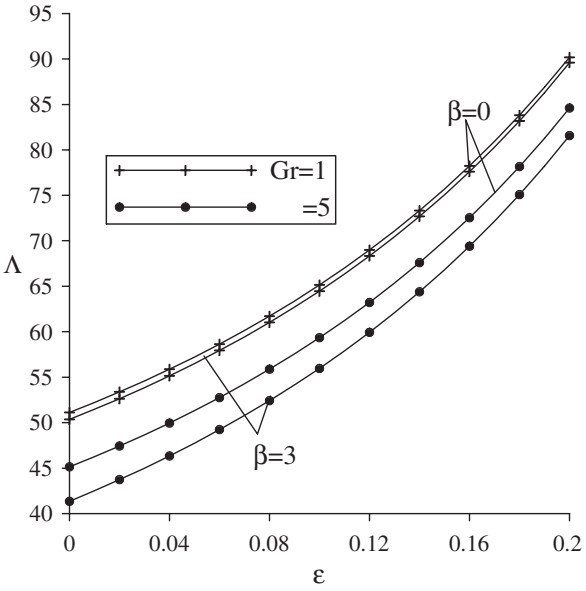

Fig. 7. Variation of longitudinal impedance versus ε for different values of β and Gr at $a = 0.1$, $m = -1$, $z_0 = 0.8$, $Q_s = 0.4$, $\alpha = 0.4$, and Pr $= 4$.

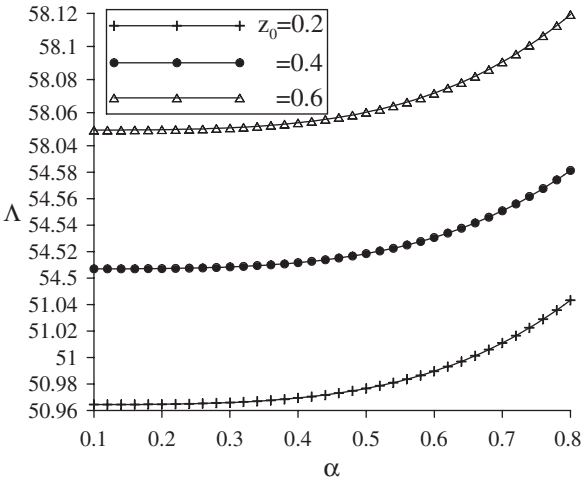

Fig. 8. Variation of longitudinal impedance versus α for different values of z_0 at $a = 0.3$, $m = -1$, $\beta = 0.5$, $Q_s = 0.5$, $\varepsilon = 0.1$, Gr $= 4$, and Pr $= 4$.

at $r = a$ to its value $m = 1$ at $r = r_2$. But the heat increases from its value $m = 1$ at $r = r_2$ to a maximum temperature at $r = 0.8$, then it decays steadily to its value $m = -1$ at $r = a$. Furthermore, the temperature θ of the fluid increases by increasing heat source parameter β. The temperature θ of the fluid versus z at $r = 0.5$ with different values of the Prandtl number Pr and the pulsatile Reynolds number α is shown in Figure 14. It is clear that the temperature θ decreases as the Prandtl number Pr and the pulsatile Reynolds num-

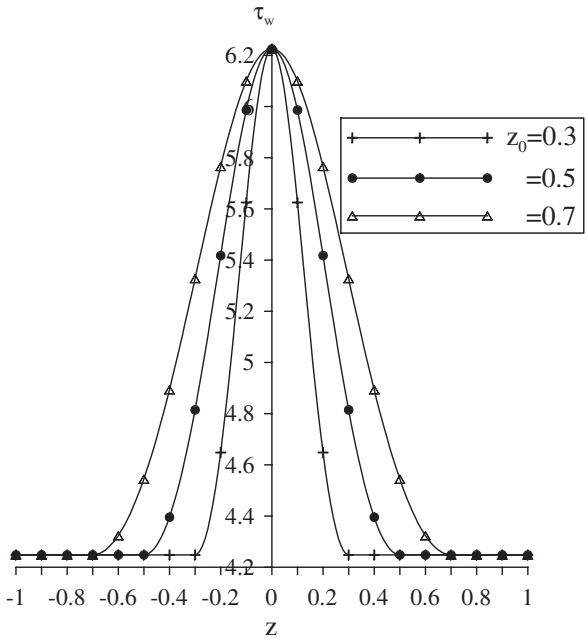

Fig. 9. Variation of wall shear stress versus z for different values of z_0 at $a = 0.3$, $m = -1$, $\alpha = 0.5$, $\beta = 0.2$, $Q_s = 0.5$, $\varepsilon = 0.1$, Gr $= 2$, Pr $= 2$, and $t = 0$.

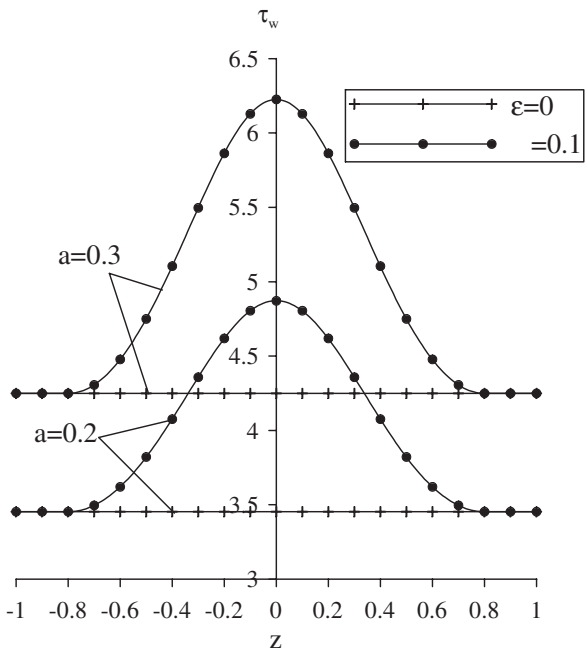

Fig. 10. Variation of wall shear stress versus z for different values of a and ε at $m = -1$, $\alpha = 0.5$, $\beta = 0.2$, $Q_s = 0.5$, $z_0 = 0.8$, Gr $= 2$, Pr $= 2$, and $t = 0$.

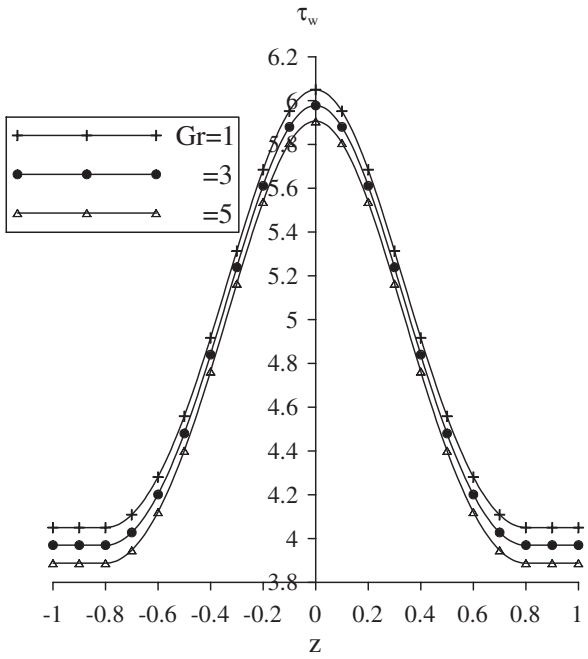

Fig. 11. Variation of wall shear stress versus z for different values of Gr at $a = 0.3$, $\varepsilon = 0.1$, $m = 2$, $\alpha = 0.5$, $\beta = 0.5$, $Q_s = 0.8$, $z_0 = 0.8$, Pr $= 2$, and $t = 0$.

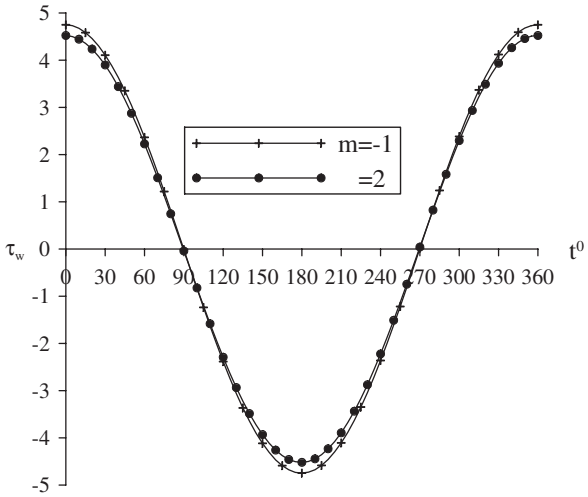

Fig. 12. Variation of wall shear stress in a time cycle of oscillation (t^0) for different values of m at $a = 0.3$, $\varepsilon = 0.1$, Gr $= 2$, $\alpha = 0.5$, $\beta = 0.5$, $Q_s = 0.8$, $z_0 = 0.8$, Pr $= 2$, and $z = 0.5$.

ber α increase. Also the figure shows that the fluid temperature θ is constant at the non-stenosis part, but in the stenosis part it decreases to the minimum value at $z = 0$. Figure 15 depicts the variation of the fluid tem-

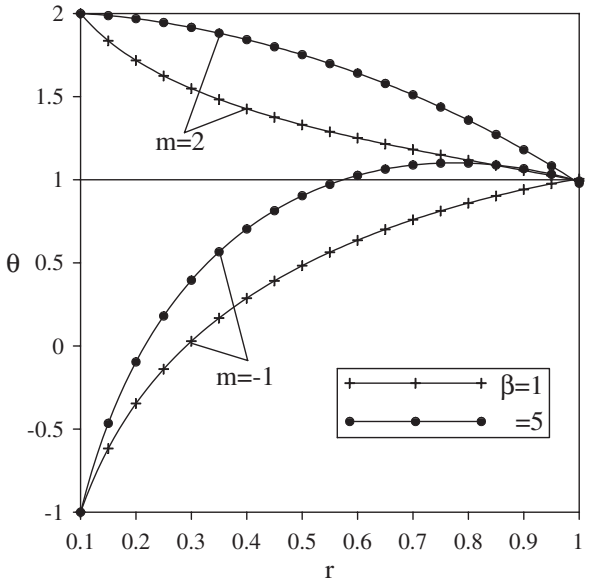

Fig. 13. Temperature distribution θ versus r for different values of m and β at $a = 0.1$, $\varepsilon = 0.01$, $\alpha = 0.9$, $z_0 = 0.8$, Pr $= 3$, $z = 0$, and $t = 0$.

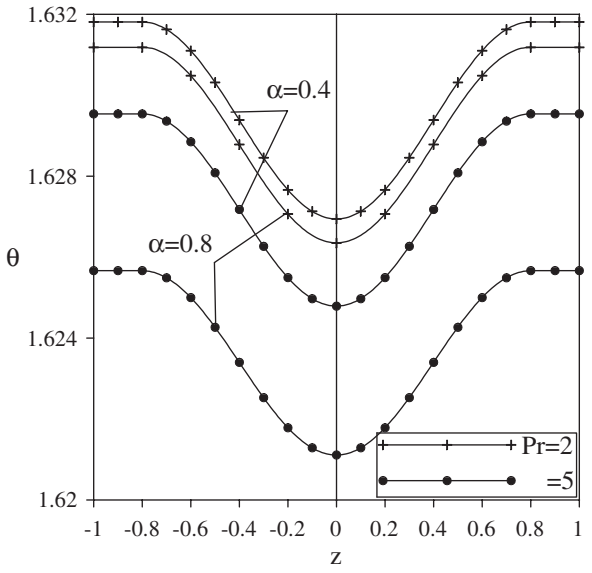

Fig. 14. Temperature distribution θ versus z for different values of α and Pr at $\beta = 1$, $a = 0.3$, $\varepsilon = 0.01$, $m = 2$, $z_0 = 0.8$, $r = 0.5$, and $t = 0$.

perature in a cycle of oscillation for different values of r. It is clear that the temperature increases as t increases from 0° to 180° and then decreases from 180° to 360°. The fluid temperature θ vanishes (equivalence

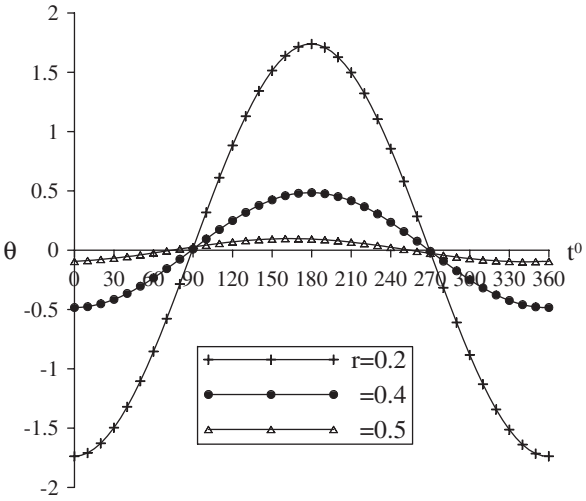

Fig. 15. Temperature distribution θ^* in a time cycle of oscillation (t^0) for different values of r at $a = 0.3$, $\varepsilon = 0.1$, $\alpha = 0.5$, $\beta = 1$, $m = -1$, $z_0 = 0.8$, Pr $= 2$, and $z = 0$.

points) at 90° and 270°. Also the figure shows that the fluid temperature θ increases as r increases in the time intervals 0° to 90° and 270° to 360° but it decreases as r increases in the time interval 90° to 270°.

5. Limitations of the Study

The present study has a number of limitations. We have assumed Newtonian fluid flow in order to simplify the mathematical model. It seems to us that the consideration of the non-Newtonian behaviour of blood would have represented an unnecessary complication (in large vessels such as the venae cavae which are typically considered here for the venous access, it is customary to adopt a Newtonian model for the blood). Arterial geometry has also been simplified in our model to be suitable for the cylindrical coordinate system. The assumption that the catheter remains at the center of the artery is unlikely in reality. Future studies will attempt to address these limitations.

6. Concluding Remarks

This work presents an analytical solution for the unsteady Newtonian fluid through a vertical constricted annulus with heat transfer. The pressure gradient, resistive impedance, wall shear stress, and temperature are calculated. The main findings can be summarized as follows:

- The presence of a catheter in a stenosed artery and the height of the stenosis increase the pressure gradient and shear stress. The pressure gradient is larger for the case with a large-diameter catheter, since a large catheter means less flow area which leads to higher flow velocity and frictional resistance. Such a result seems reasonable from the physical and medical point of view.
- The pressure gradient is constant at the inlet and increases gradually to the maximum value at the center of the stenosis at $z = 0$, after this it decreases gradually and becomes constant at the outlet.
- The impedance Λ vanishes at the center of the stenosis $z = 0$.
- The shear stress distributions are negative in some periods of time and become positive in other periods.
- In the wider part of the annulus the pressure gradient is relatively small, that is, the flow can easily pass without imposition of a large pressure gradient.
- The temperature of the fluid increases by increasing the heat source parameter.
- The fluid temperature is constant at the non-stenosis part but in the stenosis part it decreases to the minimum value at $z = 0$.
- The fluid temperature θ vanishes (equivalence points) at $t = 90^\circ$ and 270°.

Acknowledgements

Y. Abd elmaboud wishes to thank King Abdulaziz University (KAU), Saudi Arabia, for financial support. The authors are grateful to the r eferees and editor for their constructive suggestions.

[1] A. El Hakeem, A. El Naby, and A. E. M. El Misiery, Appl. Math. Comput. **128**, 19 (2002).
[2] R. Toriia, N. B. Wood, A. D. Hughes, S. A. Thom, J. Aguado-Sierra, J. E. Davies, D. P. Francis, K. H. Parker, and X. Y. Xu, J. Biomech. **40**, 2501 (2007).
[3] M. Grigioni, C. Daniele, U. Morbiducci, G. D'Avenio, G. Di Benedetto, C. Del Gaudio, and V. Barbaro, J. Biomech. **35**, 1599 (2002).
[4] J. B. Shukla, R. S. Parihar, and S. P. Gupta, B. Math. Biol. **42**, 797 (1980).
[5] L. M. Srivastava, J. Biomech. **18**, 479 (1985).
[6] D. F. Young and F. Y. Tsai, J. Biomech. **6**, 395 (1973).
[7] B. E. Morgan and D. F. Young, B. Math. Biol. **36**, 39 (1974).
[8] P. Daripa and R. K. Dash, J. Eng. Math. **42**, 1 (2002).
[9] C. Tu and M. Deville, J. Biomech. **29**, 899 (1996).
[10] P. Chaturani and R. Ponnalagar Samy, Biorheology **23**, 499 (1986).
[11] M. A. Ikbal, S. Chakravarty, K. K. L. Wong, J. Mazumdar, and P. K. Mandal, J. Comput. Appl. Math. **230**, 243 (2009).
[12] D. Srinivasacharya and D. Srikanth, C.R. Mecanique **336**, 820 (2008).
[13] Kh. S. Mekheimer and M. A. EL Kot, Chem. Eng. Commun. **197**, 1195 (2010).
[14] Kh. S. Mekheimer, M. H. Haroun, and M. A. El Kot, Can. J. Phys. **89** (2011) doi:10.1139/P10-103.
[15] Kh. S. Mekheimer and M. A. El Kot, Acta Mech. Sinica **24**, 637 (2008).
[16] Kh. S. Mekheimer and M. A. El Kot, Appl. Math. Mech. **29**, 1 (2008).
[17] R. K. Dash, G. Jayaraman, and K. N. Mehta, J. Biomech. **32**, 49 (1999).
[18] J. C. Misra and S. Chakravarty, J. Biomech. **19**, 907 (1986).
[19] L. M. Srivastava and V. P. Srivastava, Biorheology **20**, 761 (1983).
[20] D. F. Young, J. Eng. Ind. **90**, 248 (1986).